JOURNAL OF BIOMEDICAL OPTICS 4(4), 482–489 (OCTOBER 1999)

CHARACTERIZING THE COHERENCE OF BROADBAND SOURCES USING OPTICAL PHASE SPACE CONTOURS

A. Wax, S. Bali, G. A. Alphonse, and J. E. Thomas
Duke University, Physics Department, Durham, North Carolina 27708-0305

(Paper JBO-90006 received Jan. 25, 1999; revised manuscript received June 21, 1999; accepted for publication July 1, 1999.)

ABSTRACT

Advances in optical coherence tomography (OCT) rely on the availability of broadband light that is spatially coherent. We present a technique to characterize coherence properties of broadband light using optical phase-space contours in transverse momentum and position. We demonstrate that these contour plots can be directly measured by a simple heterodyne imaging scheme possessing high dynamic range (130 dB) and 0.1 fW sensitivity (for mW input beams). These phase space distributions are shown to yield quantitative information on the longitudinal and transverse coherence and the wavefront curvature of the light beam. We apply this technique to characterize the light emitted by a novel high-power extended-bandwidth superluminescent diode (SLD) recently developed at the David Sarnoff Research Center. Its performance is compared to that of standard commercially available SLDs. [S1083-3668(99)00604-8]

Keywords optical coherence; phase space distributions; optical wavefront; broadband light source; superluminescent diode; optical coherence tomography.

1 INTRODUCTION

In recent years optical coherence tomography (OCT) has emerged as an exciting noninvasive medical imaging technique.[1,2] High-resolution OCT relies on interferometry with low-coherence sources of light. The short coherence length is essential for high longitudinal (or *z*) resolution. In addition, since transverse resolution is usually achieved in OCT by focusing, the light source used must possess a high degree of spatial coherence. This is essential for efficient coupling into optical fibers and for reducing the signal-degrading component of speckle that arises from out-of-focus light.[3] Measurement of the wavefront curvature is also important, as propagation in biological samples may cause wavefront distortion. Furthermore, it is well known that in working with broadband light it is easy to introduce spectral changes and dispersion effects which degrade imaging resolution. There is clearly a need to devise simple and sensitive techniques that directly measure or monitor these optical parameters for arbitrary beams.

Another very critical issue for OCT is the availability of suitable optical sources. Light emitting diodes (LEDs) are commonly used short coherence length sources which are simple, compact, and low cost, but suffer from low output power or poor spatial coherence. Other commonly used sources are multimode lasers, which may have large output power and good spatial coherence, but may still be limited by relatively long coherence lengths.[4] Several other optical sources have also recently been tried for performing OCT.[5] There is a significant need to develop high-powered short-coherence length spatially coherent light sources that are simple, compact, and inexpensive for clinical implementations of noninvasive optical biopsy. Superluminescent diodes (SLDs) in particular are emerging as very promising candidates.[6–8] Consequently there has been a great deal of interest in developing SLDs that are broad bandwidth (40–90 nm) and high-powered (50–200 mW).[9] These SLDs are capable of providing timing resolution of tens of femtoseconds for biological imaging applications, comparable to schemes that rely on time gating.[10–12]

We have developed an optical heterodyne imaging method that obtains simultaneously both position and momentum information for the light field directly in the form of optical phase space contour plots.[13] These plots yield quantitative information on the spatial coherence, as well as the wavefront curvature. The technique was originally developed for measuring the transverse phase space distributions for monochromatic fields. A modified method has been developed for low-coherence light since changes in optical paths which occur as the position and momentum are scanned must be compensated.[14] The new method is capable of not

Permanent address of G. A. Alphonse: Sarnoff Corporation, CN 5300, Princeton, NJ 08543-5300. Address all correspondence to J. E. Thomas. Tel: 919-660-2508; Fax: 919-660-2525; E-mail: jet@phy.duke.edu

1083-3668/99/$10.00 © 1999 SPIE

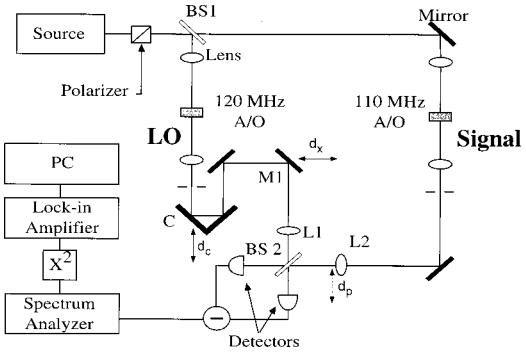

Fig. 1 Heterodyne measurements with optical beams.

only obtaining transverse distributions but also examining the longitudinal coherence properties of the light beam. Thus, it offers a simple and sensitive means of characterizing light sources. Any arbitrary beam can be characterized with this method; hence, it is applicable to studies of coherence properties of light scattered from biological samples. An added advantage of our heterodyne scheme is that by measuring the mean-*square* beat signal (instead of the mean beat amplitude as in OCT[6]), one may subtract off the LO shot noise and electronic noise in real time.[13] This achieves good noise suppression, high dynamic range (130 dB) and 0.1 fW sensitivity (using mW beams).

In this paper, we use the optical phase space method to characterize light sources. The most significant of these is the study of a new high-powered extended-bandwidth SLD developed recently at the David Sarnoff Research Center. It has a novel ''inverse-bowtie'' design[9] that enables large output power from a single chip with small transverse dimensions (few square microns). The small chip size means the light output can be expected to be reasonably spatially coherent. We find this to be true even for large driving currents. The output power and bandwidth far exceeds that of commercially available standard single-chip SLDs, thus avoiding the need to combine spectrally displaced sources[7] for imaging applications. Furthermore, in contrast to some other recently developed novel broadband SLDs,[8] it possesses a smooth spectral curve which is well-approximated by a Gaussian.

In the following sections we describe our experimental setup and the measurement of optical phase space contour plots for various sources. We outline the theory of heterodyne imaging with broadband sources,[14] and show how information about coherence properties and wavefront curvature can be extracted from the measured mean-square beat amplitude. Then data are presented and discussed.

2 EXPERIMENTAL SCHEME

The scheme of the heterodyne experiments is shown in Figure 1.[13,14] First the output from the source (in our experiments, either a He–Ne laser or a low-coherence superluminescent diode) is split into two beams, one serving as the signal, and the other as a local oscillator (LO) which is offset in relative frequency by 10 MHz with acousto-optical modulators (AO). Each of the LO and signal beams are passed through an achromatic input lens and mixed at a 50–50 beam splitter BS2. The detectors are in the Fourier plane of the input lenses L1 and L2. Technical noise is suppressed by employing a standard balanced detection system. The rms beat signal at 10 MHz is measured with an analog spectrum analyzer. An important feature of the experiments is that the analog output of the spectrum analyzer is squared using a low noise multiplier. The multiplier output is fed to a lock-in amplifier which subtracts the output with the input beam on and off.[15] Thus, the mean square electronic noise and LO shot noise are subtracted in real time. In this case, the lock-in output is directly proportional to the mean *square* beat amplitude, $|V_B|^2$. The beat amplitude $|V_B|$ is determined in the paraxial ray approximation by the spatial overlap of the LO and signal fields in the plane of the detectors. Using Fourier optics, we can relate the fields in the detector plane (D1,D2) to the fields in the source planes ($z=0$) of the input achromatic lenses L1 and L2, which have equal focal lengths $f_0=6$ cm. In order to generate phase-space contour plots of the signal field we need to scan the position of the LO beam relative to the signal beam (for position x information) and also the relative angle between the LO and signal beams (for momentum p information). It can easily be shown using Fourier optics that the x scan may be accomplished by translating mirror M1 off-axis by a variable distance d_x while the p scan may be accomplished by translating lens L2 off-axis by a variable distance d_p.[13,14] For interferometry with a broadband light source such as a SLD, the path lengths of the interfering beams need to be carefully matched to within several microns. This necessitates the incorporation of a retroreflector C (see Figure 1) to introduce a variable delay in the LO path, $2d_c$.

3 THEORY FOR HETERODYNE IMAGING WITH BROADBAND SOURCES

Heterodyning measures correlations between the LO and signal fields. To calculate the heterodyne signal we start by expressing the broadband SLD output field, in the paraxial approximation, as a sum over its Fourier components $\Omega_k=ck$ in air:

$$\mathbf{E}(\mathbf{x}_\perp,z,t)=\int d\Omega_k \mathcal{E}_k(\mathbf{x}_\perp,z)e^{-i\Omega_k(t-z/c)}, \qquad (1)$$

where the $\mathcal{E}_k$'s are assumed to be delta correlated in frequency, i.e., $\langle \mathcal{E}_k \mathcal{E}_{k'} \rangle$ is nonzero only when $\Omega_k=\Omega_{k'}$. The spatial position is expressed in terms of transverse and longitudinal coordinates given by $\mathbf{x}_\perp$ and z, respectively. The correlations between differ-

ent transverse spatial components of the field at frequency Ω_k are given by the cross-spectral density

$$\langle \mathcal{E}_k^*(\mathbf{x}_\perp, z)\mathcal{E}_{k'}(\mathbf{x}'_\perp, z)\rangle = \mathcal{W}(\mathbf{x}_\perp, \mathbf{x}'_\perp, \Omega_k)\,\delta(\Omega_k - \Omega_{k'}). \tag{2}$$

A reasonable form of $\mathcal{W}$ is afforded by assuming the SLD to be a Schell-model source.[16] Such sources are capable of producing highly collimated output beams despite being only partially coherent. A necessary requirement is that the cross-spectral density corresponding to two points $\mathbf{x}_\perp$ and $\mathbf{x}'_\perp$ depends on their separation $\mathbf{x}_\perp - \mathbf{x}'_\perp$. Thus we may write for the cross-spectral density:[16]

$$\begin{aligned}\mathcal{W}(\mathbf{x}_\perp, \mathbf{x}'_\perp, \Omega_k) \propto & \exp\left[-\frac{(\Omega_k - \Omega_{k_0})^2}{(\Delta\Omega_k)^2}\right] \\ & \times \exp\left[\frac{ik}{2R}(x_\perp^2 - x_\perp'^2)\right] \\ & \times \exp\left(-\frac{x_\perp^2 + x_\perp'^2}{4\sigma_s^2}\right) \\ & \times \exp\left[-\frac{(\mathbf{x}_\perp - \mathbf{x}'_\perp)^2}{2\sigma_g^2}\right].\end{aligned} \tag{3}$$

Since the last two terms in this model are Gaussian distributions it is known as a Gaussian Schell-model. Equation (3) is a special case of the more general form for Gaussian Schell-model beams given by Eq. (5.6-91) in Ref. 16, in that the beam parameters are specified in the detection plane as opposed to the source plane. Here, $\Omega_{k_0} = ck_0$ is the center frequency, $\Delta\Omega_k = c\Delta k$ is the $1/e$-frequency bandwidth of the source, $2\sigma_s$ is the $1/e$ intensity width of the beam, and σ_g is the transverse coherence length of the beam, which goes to ∞ for a completely spatially coherent source. Finally, R is the radius of curvature of the optical wavefront. The Gaussian Schell-model is found to adequately describe the optical beams used in the experiments, producing a good fit to the model with only small variances in the fit parameters.

As mentioned before, in our experiments the SLD output is split into two beams of equal size, one of which serves as the LO, $\mathbf{E}_{lo}$, and the other as the signal $\mathbf{E}_s$. The LO and signal beams in the planes of the achromatic lenses L1 and L2 ($z=0$), are propagated from these lenses to the detectors D1 and D2 using the Fresnel approximation and standard Fourier optics techniques. The beat signal $V_B(t)$ is determined by the spatial overlap of the LO and signal beams at the detection plane $z=f_0$. Therefore, we obtain

$$V_B = \int d^2\mathbf{x}_\perp \langle \mathbf{E}_S^*(\mathbf{x}_\perp, f_0)\mathbf{E}_{lo}(\mathbf{x}_\perp, f_0 + \Delta l)\rangle, \tag{4}$$

where the integral is over the face of the detector. $\Delta l = 2d_c - d_x$ is the additional path length of the LO field relative to the signal field for $d_p = 0$, and arises from the direct translation of optical elements (C and M1 in Figure 1). We now substitute Eqs. (2) and (3) in Eq. (4), and take into account the shift in position (d_x) and momentum (kd_p/f_0).[14] Note that both d_x and d_p are in the x plane meaning that the y integration in Eq. (4) merely yields a constant factor. Therefore, we calculate for the beat amplitude

$$\begin{aligned}V_B \propto & \exp\left[-d_x^2\left(\frac{1}{8\sigma_s^2} + \frac{1}{2\sigma_g^2}\right)\right]\int dk\, e^{ik\Delta l'} \\ & \times \exp\left[-\left(\frac{k-k_0}{\Delta k}\right)^2\right]\exp\left[-\frac{k^2\sigma_s^2}{2}\left(\frac{d_p}{f_0} + \frac{d_x}{R}\right)^2\right],\end{aligned} \tag{5}$$

where $\Delta l' \equiv \Delta l + d_p^2/2f_0 - d_x d_p/2f_0$ is the effective path increase of the LO beam relative to the signal beam. The first correction factor $d_p^2/2f_0$ is a result of the spatial shift d_p of lens L2, which shortens the signal beam's path length relative to the LO due to the curvature of the lens. The second correction factor, $-d_x d_p/2f_0$, shows that the directions of d_x and d_p are not arbitrary. They must be chosen so the sign conventions in the planes of lenses L1 and L2 agree. This is verified experimentally: When d_x and d_p are in the same direction, the path length difference between the two beams is reduced compared to shears in opposite directions which cause the path difference to increase.

As explained in the experimental section above, our heterodyne system directly measures the mean-*square* beat amplitude:

$$\begin{aligned}\langle |V_B|^2\rangle \propto & \exp\left[-d_x^2\left(\frac{1}{4\sigma_s^2} + \frac{1}{\sigma_g^2}\right)\right] \\ & \times \exp\left[-k_0^2\sigma_s^2\left(\frac{d_p}{f_0} + \frac{d_x}{R}\right)^2\right] \\ & \times \exp\left[-\left(\frac{\Delta l'}{\Delta l_B}\right)^2\right],\end{aligned} \tag{6}$$

where Δl_B represents the spatial resolution in the longitudinal direction of the heterodyne scheme, and is given by

$$\Delta l_B = \sqrt{2}/\Delta K = \frac{\sqrt{2\ln 2}}{\pi} l_c = 0.375\, l_c. \tag{7}$$

Here l_c is the longitudinal coherence length of the beam and is defined in the usual way as $l_c \equiv \lambda^2/\Delta\lambda_{\mathrm{FWHM}}$. Information on the wavefront curvature R and the transverse spatial coherence (given by the transverse coherence length σ_g) is then extracted from the heterodyne signal by measuring x-p distributions by scanning d_x and d_p. To obtain the maximum heterodyne signal, the relative path delay between the two beams is held constant at $\Delta l' = 0$ by varying d_c. Information on longitudi-

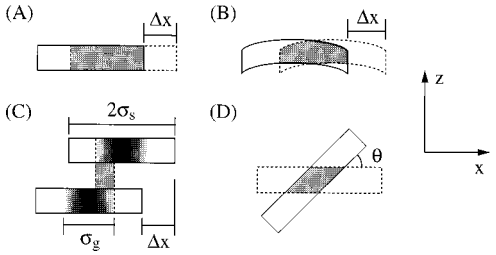

Fig. 2 Pictorial interpretation of the overlap of two identical optical wavefronts when a shear Δx or relative angle θ is introduced between them. The wavefronts are traveling in the z direction as shown, and are portrayed with finite thickness for illustrative purposes. The overlap is indicated by the shaded area: (A) for relative displacement $\Delta x = d_x$ between two planar wavefronts; (B) for the same relative displacement for two curved wavefronts the overlap is smaller; (C) for a transverse coherence length, σ_g, less than the intensity width, $2\sigma_s$, the area of coherent overlap which contributes to the heterodyne signal is further reduced; (D) for relative angle $\theta = d_p / f_0$ between the direction of propagation of the two wavefronts, assumed to be planar for simplicity.

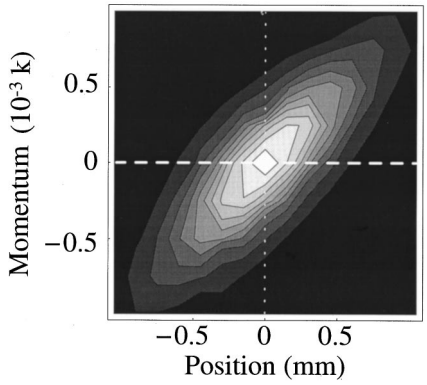

Fig. 3 Low resolution phase space contour plot of transverse position d_x vs transverse momentum p for a single-mode laser beam. Each d_x step is 150 μm and each θ step is 0.25 mrad. The ellipse is rotated, indicating beam curvature. (Note: the square shape of the central pixel is an artifact of the low resolution plot.)

nal coherence is obtained by measuring the heterodyne signal given by Eq. (6) for different path delays $\Delta l'$ with $d_x = 0$ and $d_p = 0$.

It is important to note here that the optical phase space distributions described in this paper are intimately linked to Wigner phase space distributions, thus allowing them to be placed on a firm theoretical footing. Since Wigner distributions are Fourier transform related to the mutual coherence function of the optical field,[17] they are sensitive to its coherence properties. It can be shown[13] that our heterodyne method directly measures coarse-grained Wigner distributions in position and momentum for the signal field. It has been suggested recently that coherence tomography based on measurement of Wigner distributions may yield new avenues for biophotonic imaging.[18–23]

4 RESULTS AND DISCUSSION

4.1 TRANSVERSE COHERENCE AND WAVEFRONT CURVATURE

In our case the heterodyne signal measures the interference between two identical optical wavefronts—the LO and signal beams. Figures 2(A)–2(D) depict pictorially two optical wavefronts with either a relative shear ($d_x = \Delta x$) or a relative angle $\theta = d_p / f_0$ between them. The heterodyne signal is proportional to the spatial overlap of the two wavefronts. The traveling wavefronts are drawn with finite thickness for illustrative purposes and the overlap is indicated by a shaded area. Optical phase space contours are generated by scanning d_x and d_p.

Figure 3 shows a measured phase space contour, $\langle |V_B(d_x, d_p)|^2 \rangle$ for a single-mode He–Ne laser beam. The position axis denotes the LO center position d_x. The momentum axis denotes the LO center momentum p_c in units of the optical wave vector as an angle: $\theta = p_c / k = d_p / f_0$. The clockwise rotation of the phase space ellipse is a simple consequence of the correlation between the mean momentum and position for a diverging wavefront. This is because, as explained in Ref. 13, for a shift in position away from the beam center, the mean momentum shifts in the same direction (and in the opposite direction for a converging beam). To determine the spatial width of the beam from the contour plot, we first extract a transverse momentum distribution as a function of θ for $d_x = 0$ (indicated by the vertical dotted line in Figure 3). This yields a Gaussian distribution with a $1/e$ angular width, $(\theta)_{1/e} = (d_p)_{1/e} / f_0$ of 0.375 ± 0.007 mrad. Now, setting $d_x = 0$, one finds from Eq. (6) that the $1/e$ intensity width, $2\sigma_s$, is given in terms of $(\theta)_{1/e}$ by

$$2\sigma_s = \frac{2}{k_0 (\theta)_{1/e}} = \frac{2 f_0}{k_0 (d_p)_{1/e}}. \tag{8}$$

In the case of the He–Ne beam, this yields an intensity width $2\sigma_s = 0.54$ mm which was verified by a beam profile measurement made with a diode array. On the other hand, plotting the position distribution for zero transverse momentum ($d_p = 0$, $\theta = 0$), indicated by the horizontal dashed line in Figure 3, yields a Gaussian distribution with a $1/e$ width, $(d_x)_{1/e}$, of 0.37 ± 0.005 mm. This is smaller than the measured spatial width $2\sigma_s = 0.54$ mm due to the presence of curvature in the LO and signal wavefronts. Note that for a single-mode laser beam σ_g can be safely assumed to be much larger than the spatial extent of the beam and therefore neglected. In other words, the He–Ne laser beam is spatially coherent over its entire wavefront. To illustrate the effect of curvature Figures 2(A) and 2(B) depict the effect of shear on the overlap of planar and curved wavefronts, respectively. The beat signal falls off faster for curved wavefronts as we scan d_x than if

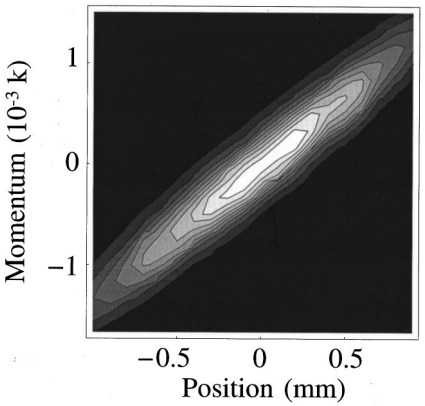

Fig. 4 Low resolution phase space contour plot of transverse position x vs transverse momentum p_x for a commercially available standard SLD made by Anritsu. Each d_x step is 100 μm and each θ step is 0.17 mrad.

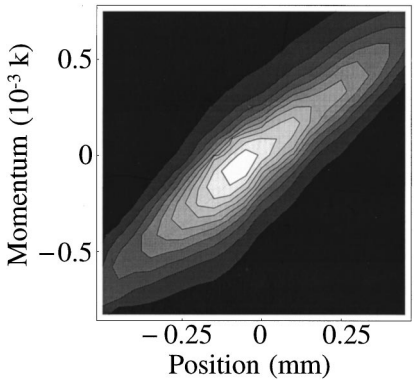

Fig. 5 High resolution phase space contour plot of transverse momentum p_x vs transverse position x for the Sarnoff SLD. Each d_x step is 50 μm and each θ step is 0.083 mrad.

the wavefronts were planar. Setting $d_p=0$, one finds from Eq. (6) that the radius of curvature R is given by

$$R=k_0\sigma_s\left(\frac{1}{(d_x)_{1/e}^2}-\frac{1}{4\sigma_s^2}-\frac{1}{\sigma_g^2}\right)^{-1/2}. \qquad (9)$$

Substituting $(d_x)_{1/e}=0.37\pm0.005$ mm, $\sigma_g \gg \sigma_s$, $2\sigma_s=0.54$ mm in Eq. (9) we deduce that the radius of curvature $R=1.36$ m.

Figure 4 shows typical phase space contours for a commercially available SLD, made by Anritsu.[24] The optical beam has been collimated using a short focal length lens and its astigmatism corrected using anamorphic prisms. The resulting beam is reduced in diameter using a reversed ×5 telescope. The Anritsu SLDs typically have a bandwidth of 10–16 nm, and a center wavelength near 852 nm. Our measurements are made at a power output level of 1.5 mW. The momentum distribution at zero transverse position is again Gaussian with a $1/e$ width $(\theta)_{1/e}=(d_p)_{1/e}/f_0=0.32\pm0.01$ mrad. Substituting this in Eq. (8) we find the intensity $1/e$ width $2\sigma_s=0.85$ mm. For zero transverse momentum, the position distribution has a Gaussian $1/e$ width $(d_x)_{1/e}=0.24\pm0.02$ mm, smaller than the calculated spatial $1/e$ width, σ_s, of 0.43 mm. This is because besides possessing curvature (like the He–Ne beam), the SLD output beams also possess a finite transverse coherence length σ_g (unlike the He–Ne beam). In other words, the heterodyne signal is reduced not only due to wavefront curvature but also because the LO and signal beams are not completely spatially coherent across their respective wavefronts. Figure 2(C) depicts pictorially the transverse coherence length σ_g for beams with planar wavefronts when σ_g is less than the spatial extent of the beam $2\sigma_s$. Only overlap of spatially coherent portions produce a heterodyne beat. To determine the value of σ_g one can eliminate R in the second exponential term of Eq. (6) by integrating both sides over d_p. This amounts to summing up all the θ values in the plot shown in Figure 4 corresponding to each value of d_x. Plotting this d_p-integrated beat signal with respect to d_x yields a Gaussian distribution with a $1/e$ width, $(D_x)_{1/e}$, of 0.83 ± 0.05 mm. Using $2\sigma_s=0.85$ mm and

$$\frac{1}{4\sigma_s^2}+\frac{1}{\sigma_g^2}=\frac{1}{(D_x)_{1/e}^2}, \qquad (10)$$

we find that $\sigma_g=4$ mm. Therefore the degree of global coherence[16] of the SLD output in any transverse cross section of the beam is $\sigma_g/\sigma_s \approx 10$. For Gaussian Schell-model beams, this quantity is invariant on propagation. We conclude that the output of the Anritsu SLD is spatially coherent. This implies that the Anritsu SLD chip is, for all practical purposes, a point-like source and its output can be focused down to a purely diffraction-limited spot for OCT applications. However, upon increasing the driving current to produce power levels higher than 1.5 mW, the longitudinal coherence properties suffer greatly as described in the next section. To complete the characterization of the transverse coherence of the Anritsu SLD we note that since both σ_g and σ_s are now known, we may use the $1/e$ width of the position distribution for $d_p=0$, i.e., $(d_x)_{1/e}=0.24\pm0.02$ mm, to deduce $R=0.78$ m from Eq. (9). The small error bars for d_x, D_x, and d_p show that the corresponding profiles are well fit by Gaussian distributions. This shows that the Gaussian Schell-model is a good description of this beam.

Figure 5 shows typical phase space contours for the high-power SLD developed at Sarnoff. The optical beam was collimated using a short focal length lens and its astigmatism corrected using cylindrical lenses to expand the beam in one dimension. The resulting beam is reduced in diameter using a reversed ×5 telescope. The Sarnoff SLDs have a bandwidth of about 40–50 nm, and a center wave-

length of 832 nm. These measurements are made at an output power of 28 mW. The maximum power levels attainable on these particular SLDs, with adequate heat sinking and with driving currents of up to 900 mA, is 50–100 mW. Proceeding as before, we first determine from the contour plot in Figure 5 the momentum distribution for zero transverse position. This curve yields a $1/e$ momentum width $(\theta)_{1/e}=(d_p)_{1/e}/f_0=0.27\pm0.02$ mrad, which when substituted in Eq. (8), yields a $1/e$ intensity width $2\sigma_s=0.98$ mm. For zero transverse momentum, the position distribution has a Gaussian $1/e$ width $(d_x)_{1/e}=0.15\pm0.01$ mm, significantly smaller than the measured spatial $1/e$ width, σ_s, of 0.49 mm. Plotting the d_p-integrated beat signal with respect to d_x yields a nominally Gaussian distribution with a $1/e$ width of $(D_x)_{1/e}=0.37\pm0.05$ mm. Substituting this and $2\sigma_s=0.98$ mm in Eq. (10), we find $\sigma_g=0.4$ mm. The radius of curvature R is then deduced from Eq. (9) to be 0.61 m. For this source the degree of global coherence is $\sigma_g/\sigma_s=0.8$, meaning the high-power SLDs output is not fully spatially coherent. While the profiles in d_x and d_p are well fit by Gaussian distributions as evidenced by the small error bars, the parameter D_x has a slightly larger error bar. This is due to the asymmetry in position distribution which can be seen in the phase space distribution for this beam (Figure 5). The Gaussian–Schell model does not account for this asymmetry. However, it provides an adequate description of the beam since D_x, d_x, and d_p are determined with only 10% errors (13.5% for D_x).

The probable reason for the decreased spatial coherence of the Sarnoff SLD is the presence of stray light near the output spot arising from high single-pass gain. This detracts from the point-like nature of the source. Work is in progress at Sarnoff to block this stray light. If only one spatially coherent area of the beam is selected using an aperture (a region of radius 0.4 mm of the 28 mW beam), the usable power would be about 4.5 mW. However, this SLD is operating with a current of 640 mA, far below its maximum recommended current of 900 mA; thus the usable power can be increased. It is also important to note that the longitudinal coherence properties of its output do not degrade as the driving current is increased, as described below.

4.2 LONGITUDINAL COHERENCE

Typical frequency profiles for the Anritsu as well as the Sarnoff SLDs, as measured with a monochromator, are Gaussian as expected. For the Anritsu SLD, centered at 852 nm, $\Delta\lambda_{FWHM}=10.3$ nm. This corresponds to a longitudinal coherence length, $l_c=70.3\,\mu$m which, from Eq. (7), implies for our heterodyne scheme a longitudinal spatial resolution of $\Delta l_B=26.4\pm2.6\,\mu$m. Note that these measurements were made for a power output of 1.5 mW at a driving current of 85 mA. Although increasing the drive current results in increased power, we found that the longitudinal coherence characteristics of these diodes begin to degrade for currents higher than 85 mA.

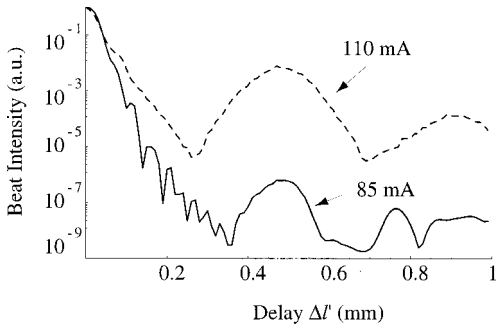

Fig. 6 Mean-square heterodyne signal plotted as a function of effective path delay $\Delta l'$ for the Anritsu SLD at two different driving currents. The power output at 85 mA is 1.5 mW, and at 110 mA is almost 4 mW. $\Delta l'$ is defined as used in Eq. (5). Note the presence of significant secondary peaks in addition to the primary signal at zero path delay.

To examine this degradation sensitively, we exploit the high dynamic range of our heterodyne imaging setup. Figure 6 shows the mean-square beat signal, described by Eq. (6), as a function of longitudinal path delay $\Delta l'$ at two different driving currents. These longitudinal coherence profiles are obtained by scanning d_c while holding d_x, d_p fixed at zero. Besides the primary beat signal, one notices the presence of secondary peaks. These peaks are considerably smaller than the primary peak (more than 6 orders of magnitude smaller) for the low output power. However, they are only a factor 100 smaller for higher output powers, and repeat every 0.45 mm. The periodicity of the secondary peaks suggests multiple reflections occurring within the diode package itself at higher currents, as explained below.

The frequency profile of the Sarnoff SLD is centered at 832 nm and has a bandwidth $\Delta\lambda_{FWHM}=44$ nm yielding a longitudinal coherence length l_c of 15.7 μm. Therefore, from Eq. (7), we find the heterodyne spatial resolution Δl_B should be 5.9 μm (with a corresponding temporal resolution of 19.7 fs). However, our optics do not have enough bandwidth for this source and limit us to a measured value for Δl_B of $7.4\pm0.4\,\mu$m. Figure 7 shows the typical mean square beat signal as a function of path delay for a Sarnoff diode operated, as for the investigation of transverse coherence, at 640 mA with a power output of 28 mW. We see that the secondary peaks are largely suppressed and are a factor 10^8 smaller than the primary heterodyne signal. This scan is extended to 3 mm to demonstrate that the Sarnoff SLD does not exhibit significant secondary modes even at longer path delays. The ripple structure seen in the path delay scan is due to the short coherence length of the source accentuating the starting and stopping of the translators. This can be corrected by moving the transla-

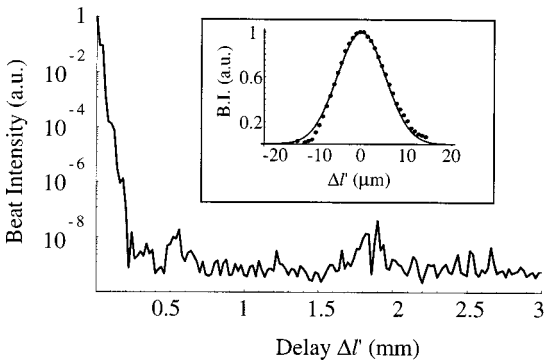

Fig. 7 Mean-square heterodyne signal plotted as a function of effective path delay $\Delta l'$ for the Sarnoff SLD driven at 640 mA with an output power level of 28 mW. $\Delta l'$ is defined as used in Eq. (5). The secondary peaks are largely suppressed. Inset: High resolution plot for short path delay.

tors at slower velocities. A scan taken with slower translator velocity is shown in the inset of Figure 7. The slower velocity with high resolution limits the scan to a shorter total path delay. The scan shown in the inset was used to measure the value of $\Delta l_B = 7.4\,\mu$m.

The secondary peaks seen in the case of the Anritsu SLD are extremely undesirable for imaging applications that rely on detecting heterodyne signals. We have used optical phase space tomography with monochromatic and broadband sources to probe the light scattering characteristics of turbid media.[18–21] We rely on the short coherence length of our broadband source to selectively examine the low-order scattered light at small differences in path length from the ballistic light. If the light from undesired secondary modes in the diode package happens to be also longitudinally phase matched with the scattered light, it strongly affects the detected beat intensity and severely degrades longitudinal resolution.

The cause of the secondary peaks in Figure 6 is probably undesired longitudinal modes. A narrowband laser may possess a single transverse and longitudinal mode, but a broadband source such as a SLD obviously does not. The SLD is operating in several longitudinal modes at different optical frequencies, but a very small portion of the total light output is reflected back through the gain medium as in a laser. For the Sarnoff SLD the single-pass gain is as high as 40–50 dB, therefore it does not take much reflection to cause undesired copropagating modes. They can cause spectral modulation or ''ripples'' to appear in the optical frequency spectrum that reduce the spectral width and may even cause laser oscillations. In fact, with a 50 dB single-pass gain, the reflection must be less than −70 dB in order to suppress the ripples below 1%. The ripples tend to be more pronounced at higher driving currents. This is the reason that increasing the current on the Anritsu SLD increases its power output but severely affects its coherence properties. On the other hand, spectral ripples in the Sarnoff SLD have been kept at the 1% level even at high driving currents, thus leaving its longitudinal coherence properties unchanged.

5 CONCLUSION

In conclusion, we have demonstrated the utility of our heterodyne optical phase space method[13,14] in simultaneously measuring several important optical properties of novel broadband sources. Optical phase space contours are generated which are shown to yield quantitative information about the longitudinal and transverse coherence as well as the curvature of the optical wavefront. The technique has high dynamic range (130 dB) and 0.1 femtoWatt sensitivity (with mW input beams) and hence has broad potential applicability to the field of biophotonic imaging. We have characterized the coherence properties of a novel high-power superluminescent diode that has great potential for medical imaging tools. This source and the phase space tomography method described here currently are being applied to study the phase space distributions of low-order scattered light for application to imaging through turbid media.[18–21] Work is in progress at Sarnoff to further improve the SLD's spatial coherence properties and also extend its bandwidth.

Acknowledgments

The authors gratefully acknowledge invaluable experimental help from K. F. Lee. They also thank Professor Dr. Christoph Hitzenberger for communicating a preprint of Ref. 8 to us prior to publication. This research has been supported by the National Institute of Health.

REFERENCES

1. A. F. Fercher, ''Optical coherence tomography,'' *J. Biomed. Opt.* **1**, 157–173 (1996).
2. J. A. Izatt, M. D. Kulkarni, K. Kobayashi, M. S. Sivak, J. K. Barton, and A. J. Welch, ''Optical coherence tomography for biodiagnostics,'' *Opt. Photonics News* **8**(5), 41–47 (1997).
3. J. M. Schmitt, S. H. Xiang, and K. M. Yung, ''Speckle in optical coherence tomography,'' *J. Biomed. Opt.* **4**(1), 95–105 (1999).
4. D. N. Wang, Y. N. Ning, K. T. V. Grattan, A. W. Palmer, and K. Weir, ''Optimized multiwavelength combination sources for interferometric use,'' *Appl. Opt.* **3**, 7326–7333 (1994).
5. B. E. Bouma, L. E. Nelson, G. J. Tearney, D. J. Jones, M. E. Brezinski, and J. G. Fujimoto, ''Optical coherence tomographic imaging of human tissue at 1.55 μm and 1.81 μm using Er- and Tm-doped fiber sources,'' *J. Biomed. Opt.* **3**, 76–79 (1998); and references therein.
6. D. Huang, E. A. Swanson, C. P. Lin, J. S. Schuman, C. A. Puliafito, and J. G. Fujimoto, ''Optical coherence tomography,'' *Science* **254**, 1178–1181 (1991).
7. A. Baumgartner, C. K. Hitzenberger, H. Sattmann, W. Drexler, and A. F. Fercher, ''Signal and resolution enhancements in dual beam optical coherence tomography of the human eye,'' *J. Biomed. Opt.* **3**(1), 45–54 (1999).
8. C. K. Hitzenberger, A. Baumgartner, W. Drexler, and A. F. Fercher, ''Dispersion effects in partial coherence interferometry: implication for intraocular ranging,'' *J. Biomed. Opt.* **4**(1), 144–151 (1999).

9. G. A. Alphonse, N. Morris, M. G. Harvey, D. B. Gilbert, and J. C. Connolly, ''New High-Power Single-Mode Superluminescent Diode with Low Spectral Modulation'' in *Conference on Lasers and Electro-Optics*, Vol. 9, pp. 107–108, OSA Technical Digest Series, Optical Society of America, Washington, DC (1996).
10. L. Wang, P. P. Ho, C. Liu, G. Zhang, and R. R. Alfano, ''Ballistic 2-D imaging through scattering walls using an ultrafast optical Kerr gate,'' *Science* **253**, 769–771 (1991).
11. J. Wu, Y. Wang, L. Perelman, I. Itzkan, R. R. Dasari, and M. S. Feld, ''Time-resolved multichannel imaging of fluorescent objects embedded in turbid media,'' *Opt. Lett.* **20**, 489–491 (1995).
12. M. S. Patterson, B. Chance, and B. C. Wilson, ''Time resolved reflectance and transmittance for the non-invasive measurement of tissue optical properties,'' *Appl. Opt.* **28**, 2331–2336 (1989).
13. A. Wax and J. E. Thomas, ''Optical heterodyne imaging and Wigner phase space distributions,'' *Opt. Lett.* **21**, 1427–1429 (1996).
14. A. Wax, S. Bali, and J. E. Thomas, ''Optical phase space distributions for low-coherence light'' *Opt. Lett.* **24**, 1188 (1999).
15. Related methods have been used previously. See, for example, G. L. Abbas, V. W. S. Chan, and T. K. Yee, ''A dual-detector optical heterodyne receiver for local oscillator noise suppression,'' *J. Lightwave Technol.* **3**, 1110 (1985).
16. L. Mandel and E. Wolf, *Coherence and Quantum Optics*, Cambridge University Press (1995).
17. E. P. Wigner, ''On the quantum correction for thermodynamic equilibrium,'' *Phys. Rev.* **40**, 749–759 (1932); M. Hillery, R. F. O'Connel, M. O. Scully, and E. P. Wigner, ''Distribution functions in physics: Fundamentals,'' *Phys. Rev. B* **106**, 121–167 (1984).
18. A. Wax and J. E. Thomas, ''Measurement of smoothed Wigner phase space distributions for small angle scattering in a turbid medium,'' *J. Opt. Soc. Am. A* **15**, 1896–1908 (1998).
19. A. Wax and J. E. Thomas, ''Heterodyne measurement of Wigner phase space distributions in turbid media,'' in *Advances in Optical Imaging and Photon Migration*, R. R. Alfano and J. G. Fujimoto, Eds., pp. 238–242, Optical Society of America, Washington, DC (1996).
20. A. Wax and J. E. Thomas, ''Measurement of smoothed Wigner phase space distributions for low coherence light in multiple scattering media,'' in *Coherence Domain Optical Methods in Biomedical Science and Clinical Applications III*, V. V. Tuchin and J. A. Izatt, Eds., *Proc. SPIE* **3598**, 2–9 (1999).
21. A. Wax and J. E. Thomas, ''Measurement of smoothed Wigner phase space distributions for coherence tomography,'' in *Saratov Fall Meeting 98: Light Scattering Technologies for Mechanics, Biomedicine and Material Science*, V. V. Tuchin, V. P. Ryabukho, and D. A. Zimnyakov, Eds., *Proc. SPIE* **3726**, 494–501 (1999).
22. M. G. Raymer, C. Cheng, D. M. Toloudis, M. Anderson, and M. Beck, ''Propagation of Wigner coherence functions in multiple scattering media,'' private communication (1995).
23. S. John, G. Pang, and Y. Yang, ''Optical coherence propagation and imaging in a multiple scattering medium,'' *J. Biomed. Opt.* **1**, 180–191 (1996).
24. Anritsu model No. SD1S101C.